

Title No. 115-S102

Effects of Alkali-Silica Reaction on Concrete Squat Shear Walls

by Farhad Habibi, Shamim A. Sheikh, Frank Vecchio, and Daman K. Panesar

Results from testing two shear walls made with normal concrete and three walls with concrete containing reactive aggregate causing alkali-silica reaction (ASR) are presented. To accelerate the ASR and deterioration of the concrete, the walls were stored in an environmental chamber, specially constructed with the capacity to store large specimens in a controlled high-temperature and high-humidity condition. Shear walls were tested in three stages to investigate the effect of ASR over time. These walls were tested under reversed cyclic lateral loads while at the same time subjected to constant axial load simulating earthquake loads. Small companion specimens revealed that ASR caused free expansion of approximately 0.23%, but the load capacity of the walls was not adversely affected. The performance of the walls, however, deteriorated significantly over time with respect to ductility and energy dissipation capacity. The absorbed strain energy capacity of the ASR shear wall at full exhaustion was approximately 25% of that of the regular concrete wall and the displacement ductility was reduced by approximately 30% due to ASR.

Keywords: alkali-silica reaction; nuclear power plants; reinforced concrete; seismic performance; shear capacity; squat shear wall.

INTRODUCTION

Alkali-silica reaction (ASR) is a common form of concrete degradation mechanism in many structures such as bridges, dams, and roadways. This phenomenon involves a chemical reaction between reactive aggregate and the alkali hydroxides in portland cement in the presence of sufficient moisture. Recently, this problem was identified in some nuclear power plants in North America. As an example, the license extension of Seabrook Station nuclear power plant has been delayed because of the discovery of concrete degradation due to ASR in four buildings.¹ The Gentilly-2 nuclear power plant in Canada has been shut down for similar reasons. Consequently, ASR deterioration in nuclear power plants has become a concern in terms of serviceability and remaining life expectancy. ASR takes years to develop. Although its mechanism and chemistry are well understood, its effects on the behavior of structural elements are not. Several studies have been done on small-scale plain concrete specimens to quantify the effect of ASR on concrete. However, there are few results available in the literature on the effects of ASR on the behavior of large-size reinforced concrete structures. Therefore, numerous uncertainties and questions arise regarding nuclear containment structures affected by ASR.

Among the first researchers in this area, Kobayashi et al.² tested 10 prestressed concrete beams. One nonreactive concrete mixture and two mixtures with different degrees of reactivity were used. All the beams had similar

geometry and were post-tensioned after being cured for 28 days in a chamber with a temperature of 20°C (73.4°F) and a relative humidity of 80%. Then, the specimens were cured under the accelerated condition for up to 405 days. Tensile strength and modulus of elasticity of the beams with ASR concrete showed a noticeable reduction. Beams were tested under four-point loading with simply supported boundary conditions. Results from these tests showed that the flexural strength and deflection of the beams affected by ASR were within 10% of nonreactive concrete beams, even when the expansive strain in vertical stirrup exceeded 1000×10^{-6} and many longitudinal cracks occurred. Fan and Hanson³ also tested six reinforced concrete beams, of which three were cast with nonreactive aggregate and three with reactive aggregate. These specimens were kept in an alkali solution for 1 year under controlled conditions before testing. At the age of 1 year, the longitudinal expansion of the top of the beams was between 800 and 1700 microstrain, depending on the amount of reinforcement used in each beam. All beams were tested to failure using four-point loading. The flexural capacity of the ASR specimens was found to be almost the same as the capacity of the normal concrete beams.

Reactor containments are designed to withstand major seismic loads. Thus, one of the main concerns about ASR is its effects on the performance of concrete structures under reversed cyclic loading simulating seismic effects. Deschenes et al.⁴ investigated the effect of ASR on nominal shear strength capacity of deep beams. Six structurally identical specimens were constructed where four were cast with reactive concrete and two with nonreactive concrete. Results revealed that the shear capacity of the deep beams was not affected by the deterioration caused by ASR. In fact, the nominal shear capacity of the ASR beams exceeded that of beams not affected by ASR. This experiment showed that confinement plays a critical role in the maintenance of structural integrity as any potential loss of material strength due to ASR was offset by the compressive stress imposed by the shear reinforcement.

Shear walls are commonly used structural elements to resist lateral loads such as earthquake. A survey of the literature also shows a common use of shear wall specimens to study the member behavior under shear. To investigate the

ACI Structural Journal, V. 115, No. 5, September 2018.
MS No. S-2017-331.R1, doi: 10.14359/51702238, was received September 6, 2017, and reviewed under Institute publication policies. Copyright © 2018, American Concrete Institute. All rights reserved, including the making of copies unless permission is obtained from the copyright proprietors. Pertinent discussion including author's closure, if any, will be published ten months from this journal's date if the discussion is received within four months of the paper's print publication.

shear behavior of concrete squat shear walls affected by ASR, a research program was undertaken at the University of Toronto with the sponsorship of the Canadian Nuclear Safety Commission (CNSC). As a part of this project, six squat shear wall specimens were constructed: four used reactive (ASR) concrete and two were constructed with normal concrete. Five of these wall specimens were structurally tested to failure. One ASR shear wall was used for material level study and nondestructive testing. Squat shear walls were chosen to minimize the flexural effects so that the behavior of the wall specimens will be dominated mostly by shear loads. In addition, to further evaluate and compare the behavior of the squat shear walls, the geometry and the reinforcement details of the six wall specimens were identical and similar to those of the nonreactive wall specimens tested by Bouchon et al.⁵

RESEARCH SIGNIFICANCE

Among all the available studies on the effects of ASR on concrete, only a few focused on the effect of ASR on reinforced concrete specimens. Information on the effect of ASR on shear behavior of reinforced concrete members is even scarcer. Large-scale reinforced concrete squat shear walls tested under reverse cyclic loading and constant axial load can provide a better indication of shear strength and shear response of structural members that undergo ASR. This paper presents results from the structural tests of five shear walls of which three were constructed with ASR concrete and the other two with regular concrete. The goal of this research is to contribute to a better understanding of the long-term impact of ASR on the health of reinforced concrete structures and their useful life.

EXPERIMENTAL INVESTIGATION

Because the focus of this experimental program was to investigate the effects of alkali-silica reaction on the shear behavior of reinforced concrete structures, similar squat shear walls were constructed using both regular and ASR concretes for this study. CSA A23.3-14⁶ and ACI 349-13⁷ define squat walls as having vertical height (h_w) to horizontal length (l_w) ratio equal to or less than 2. Two regular concrete and four ASR concrete shear wall specimens were constructed along with several control specimens, including 21 cylinders, six modulus of rupture (MOR) beams, three expansion prisms, and six dog-bone specimens for each type of concrete mixture to monitor the material properties over time. To examine the shear performance of these walls during an earthquake, it was decided to test them under reverse lateral cyclic displacements and axial load.

Test phases

One of the most common characteristics of ASR is cracking of the concrete. These cracks first develop in reactive aggregates and then propagate to the paste and eventually become visible on the surface of the concrete.⁸ In this experimental program, cracks are used as a means of assessing damage to the shear walls over time. Three phases were thus planned for the testing of the shear walls: early stage, intermediate stage, and exhaustion stage. The stage at which the ASR

cracks are visible on any part of the specimen is called early stage. Intermediate stage refers to the stage when cracking is extensive and cracks are visible throughout the entire specimen. Finally, the exhaustion stage refers to the stage when concrete expansion has been exhausted and no significant further expansion is expected.

Acceleration chamber

Under normal circumstances, the effects of ASR on structures are visible only after 10 or more years of service, depending on the availability of moisture and the variation of temperature.⁹ The reaction can be accelerated under high temperature and high humidity.¹⁰ To accelerate the effects of ASR on the shear walls and other control specimens, this project also involved construction of an acceleration chamber capable of maintaining temperatures up to 80°C (176°F) and near 100% relative humidity. The chamber provided a clear space of 5.6 x 3.4 m (18.4 x 11.2 ft) with height clearance of 2.2 m (7.2 ft). Three heaters and a fan capable of creating humidity using a fog system were installed inside the room. Both the temperature and the humidity of the room was constantly monitored using six digital temperature sensors and a humidity sensor. Data from these sensors were then displayed on the control unit that was installed outside of the room. All the shear walls and specimens were moved to the chamber 48 days after they were constructed. In this paper, the age of shear walls and specimen refers to the age of shear walls and specimens since they were cast.

The system could maintain the temperature within $\pm 0.5^\circ\text{C}$ (0.9°F) of target temperature. All the specimens, including shear walls and small control specimens, placed in the chamber were monitored every month to evaluate the damage caused by the ASR. Acceleration methods recommended by ASTM,¹¹ CSA,¹² and RILEM¹³ suggest 38°C (100°F) curing temperature for the ASR specimens. The ASR reaction at this temperature usually takes approximately 2 years to reach its exhaustion level. Considering the size of the shear wall specimens, the exhaustion would take even longer, perhaps 5 or 6 years.

Researchers have tried to increase the temperature to 60°C (140°F) to further accelerate the ASR in concrete.^{14,15} However, many problems arose, including reduced expansion compared to when it was exposed to 38°C (100°F).^{16,17} Based on the findings by Folliard et al.¹⁷ and Gautam,¹⁰ it was suggested that the accelerating temperature for investigating the large-scale specimens without compromising ASR in the concrete, should be limited to 50°C (122°F). Therefore, the temperature of the chamber was maintained at 50°C (122°F) with a relative humidity of at least 95%.

Concrete mixture

The concrete mixture design for the shear walls and the control specimens was done according to the ASTM C1293¹¹ standard. The coarse aggregate was sieved and graded to meet the gradation requirements as per ASTM C1293.¹¹ Mixture designs for both ASR and regular concretes are shown in Table 1. In the ASR concrete, only the coarse aggregate was reactive. Sand used in both regular and ASR concretes was tested for reactivity to ensure that it did not

Table 1—Mixture design of ASR and regular concrete

	ASR concrete	Regular concrete
Total concrete volume, L (gal.)	3500 (925)	2000 (528)
Total mass, kg (lb)	8539 (18,824)	4879 (10,757)
Cement, kg (lb)	1470 (3241)	840 (1852)
Coarse aggregate, kg (lb)	3932 (8668)	2247 (4953)
Water, L (gal.)	647 (171)	390 (103)
Sand, kg (lb)	2490 (5489)	1423 (3137)
Alkali pallet, kg (lb)	3.8 (8.4)	2.2 (4.9)
High-range water-reducing admixture, L (gal.)	12.0 (3.2)	7.0 (1.8)

contribute to the expansion of the concrete. Except for the type of coarse aggregate used, the mixture design is identical for both ASR and regular concretes with one minor difference. To increase the workability and flowability, 20 L (5.3 gal.) of water was added to the truck containing regular concrete on site, which is included in the mixture shown in Table 1. This addition of water is not expected to affect the properties of the concrete significantly.

Test specimens

Six shear wall specimens were designed and cast using the two types of concrete discussed above. In addition, numerous control specimens were also cast, which included 42 cylinders, 12 modulus of rupture (MOR) beams, six expansion prisms, and 12 dog-bones. In the design of the shear wall specimens, three regions were considered: the wall panel and two columns acting as boundary elements at each end of the panel; the foundation beam; and the top beam. All six wall specimens were cast on one day and casting was carried out in a way to avoid cold joints.

The main variables investigated in this test program were the type of the concrete and the age of the specimens. The geometry and the reinforcement details for all six shear wall specimens were kept identical and were based on the design of the wall specimens tested by Bouchon et al.⁵ Figure 1 shows the geometry of the shear walls.

In the wall panel, one layer of reinforcement was used in both vertical and horizontal directions, providing reinforcement ratios of 0.77% and 0.80%, respectively. The arrangement of the reinforcement was such that the vertical bars were placed in the center of the panel, creating a clear cover of 34 mm (1.34 in.) for the horizontal reinforcement and 45 mm (1.77 in.) for the vertical reinforcements. All the bars in the panel were spaced uniformly.

The panels were 1300 mm (51.18 in.) long and 750 mm (29.52 in.) high with a thickness of 101 mm (4 in.). Boundary elements, foundation, and the top beam were designed with a high reinforcement ratio to prevent any premature failure of a specimen in those regions before the wall panel failure. The reinforcement for the boundary elements was designed using vertical bars and stirrups with 45-degree hooks. This provided 0.67%, 2.10%, and 0.44% reinforcement ratio in the horizontal direction, vertical direction, and out-of-plane direction, respectively. The columns at the ends were

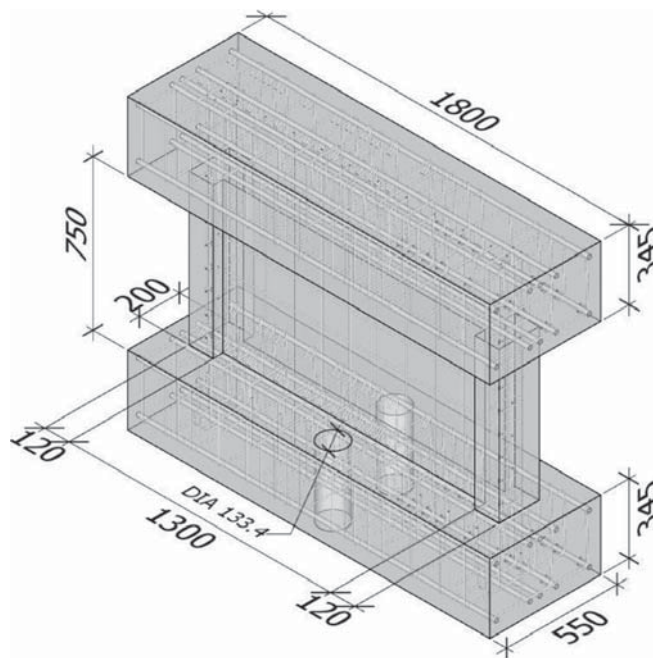


Fig. 1—Geometry of shear walls. (Note: All dimensions in mm.; 1 mm = 0.0394 in.)

120 x 200 mm (4.7 x 7.9 in.) in cross section and 750 mm (29.52 in.) long. Both top beam and the foundation beam were designed using similar reinforcement ratio and geometry. The top beam and the foundation beam were 1800 mm (71 in.) long with a cross section of 345 x 550 mm (13.6 x 21.6 in.) and a reinforcement ratio of 2.00% in all three directions. All the vertical reinforcements from the panel, and the boundary elements were extended to the foundation beam and terminated with 180-degree hooks. Refer to Fig. 2 for reinforcement details.

Two types of strain gauges were used on reinforcing steel bars to allow continuous monitoring of the behavior of the specimens through the aging process. It was also hoped that these strain gauges would provide critical information for strain in reinforcing bars during structural testing. However, during the curing process, most of these strain gauges did not last through the hot and humid conditions of the acceleration chamber and only three and five strain gauges were functioning in REG B and ASR B2 shear walls, respectively, at the time of testing in the last phase. Locations of the strain gauges used on each specimen are shown in Fig. 3. As seen, beside the reinforcing bars, strain gauges were also placed on the surface of concrete to monitor the behavior of specimens on the outer surface. These strain gauges were helpful in ensuring that the axial load was evenly applied on the specimens.

Test setup and instrumentation

Each shear wall specimen was anchored and post-tensioned to the ground using two 76.2 mm (3 in.) diameter bolts. These bolts were inserted through the steel sleeve in the holes located at midlength of the bottom beam on either side, as shown in Fig. 2. The gap between the bolts and the steel sleeves were filled with custom-made steel collars that were placed through the entire height of the bottom beam. The shear wall's bottom beam was restrained on both sides

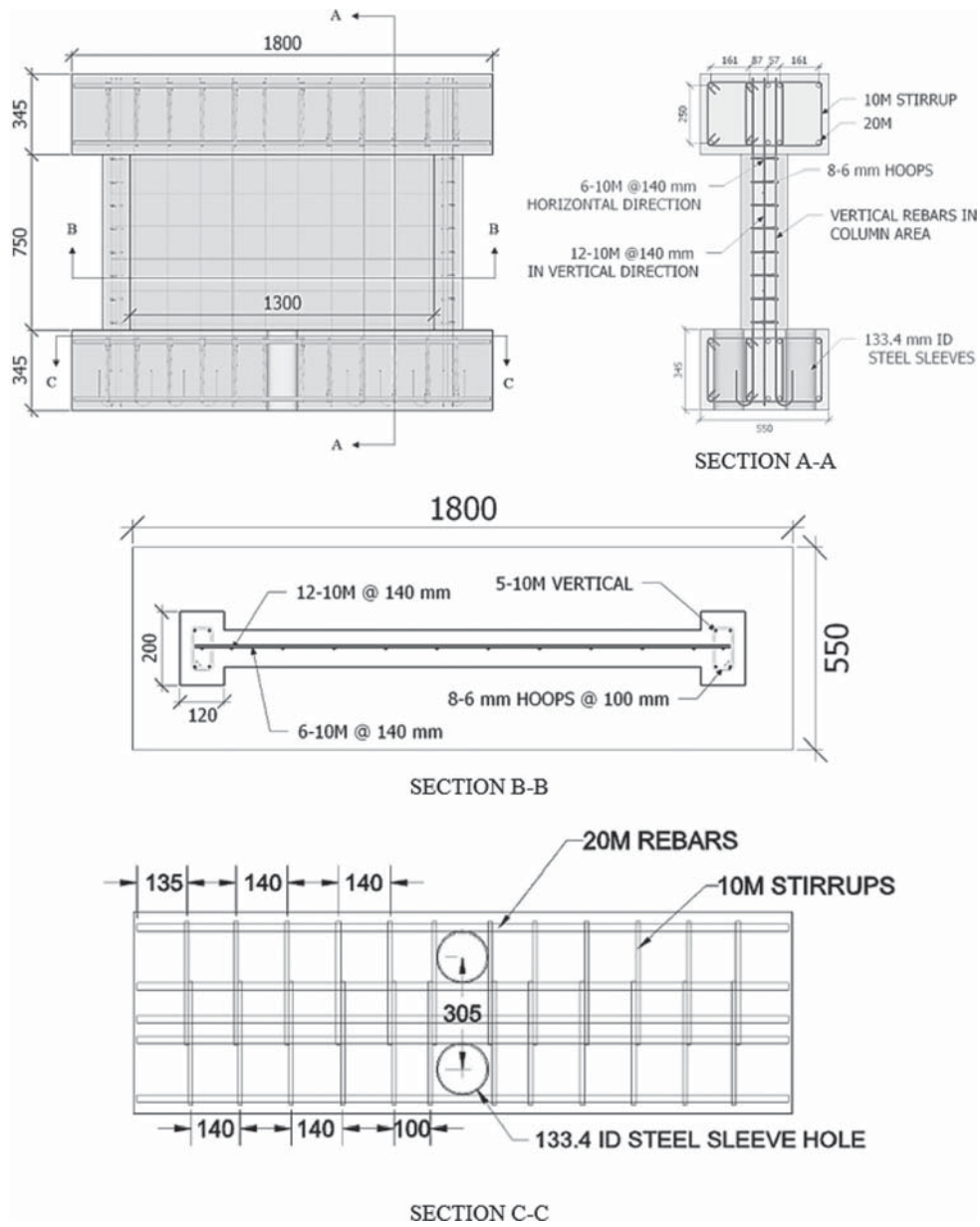


Fig. 2—Reinforcement details. (Note: All dimensions in mm; 1 mm = 0.0394 in.)

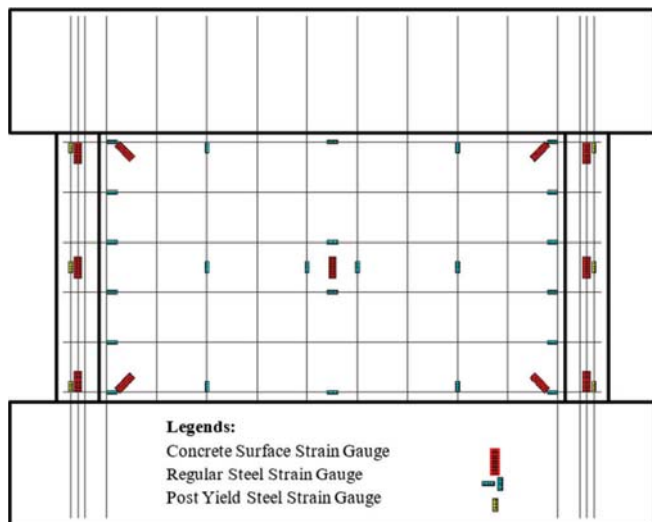


Fig. 3—Location of strain gauges.

to prevent any slippage during the tests. Based on the analysis, which was carried out using the software VecTor2,¹⁸ the ultimate capacity of the shear walls was predicted to be approximately 1200 to 1300 kN (270 to 292 kip). It was therefore decided to use two actuators with capacity of 1000 kN (225 kip) each working simultaneously. Each actuator was supported by a frame at each end of the wall specimen and a small hydraulic jack placed at the middle point of each actuator (Fig. 4). This support system allowed the actuator to move freely to allow shear deformation of the specimen. Moreover, an axial force was applied on the wall, using a hydraulic jack. With the help of servo-valves, load cells, and a control software, this jack was able to maintain a constant axial load of 800 kN (180 kip) throughout the test. Figure 4 shows a sketch of the entire test setup.

The lateral load was applied by imposing displacements on the shear walls. To simulate the effect of seismic loading, incremental reverse cyclic displacements were imposed on the walls. A series of linear voltage differential transducers

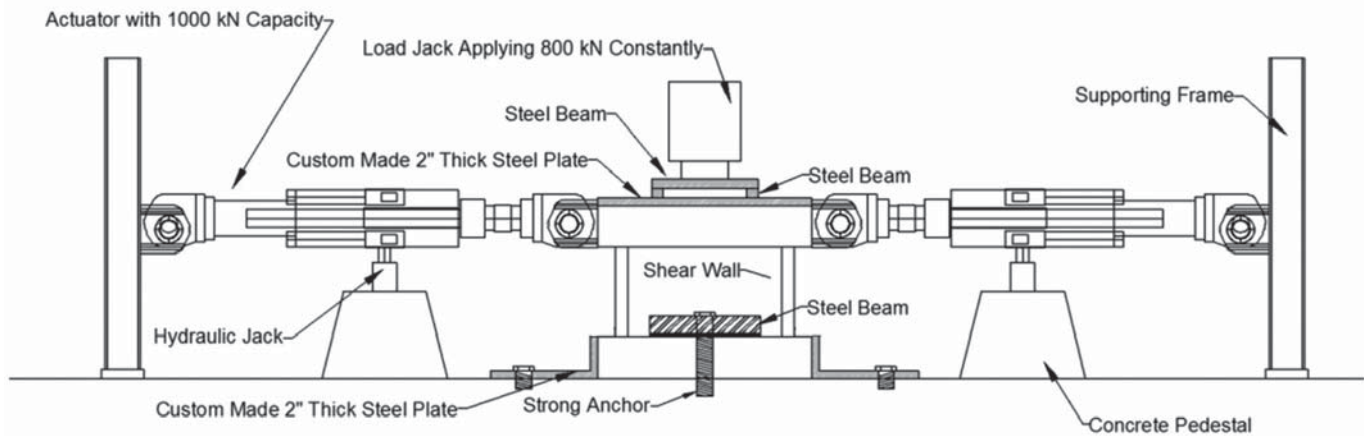


Fig. 4—Test setup. (Note: 1 kN = 0.225 kip; 1 in. = 25.4 mm.)

(LVDTs) and also the displacement transducers in the two actuators were used to control the lateral displacement of the walls. Figure 5 shows the location of the LVDTs. One LVDT was attached to an A-frame to directly measure the displacement at the vertical centerline of the wall at the bottom of the top beam with respect to the top of the bottom beam. Two LVDTs were placed on each side of the boundary elements—one at the top and the other at the bottom. Finally, one LVDT was placed at the center of the bottom beam on each side to measure any slippage of the bottom beam with respect to the strong floor. At each stage of loading, the lateral displacement captured from the LVDT attached to the A-frame was compared against the relative displacement between the four LVDTs attached to boundary elements and displacement readings from actuator's transducers to check any error in readings. After applying the geometric corrections to account for the height difference between LVDTs, the relative displacement readings in the bottom and the top LVDTs (TW-W and BW-W; TW-E and BW-E) showed consistency throughout the test for all five specimens with respect to the A-frame reading.

Loading protocol

As mentioned previously, the shear walls were subjected to reverse cyclic lateral displacement-controlled loadings. The force-displacement plot was obtained using the summation of the forces from both actuators against the displacement on top of the shear wall panel (bottom of the top beam) with respect to the bottom of the shear wall panel (top of the lower beam). The rate of loading began with 0.005 mm/s and was increased to a maximum of 0.15 mm/s (0.006 in./s) as cycles progressed. The first two cycles applied 0.2 mm (0.008 in.) lateral displacement in the plane of the wall in each direction and the subsequent planned cycles were at maximum displacements of 0.4, 0.6, 0.8, 1, 1.4, 1.8, 2, 2.5, 3, 4, 4.5, 5.5, 6, 7, and 8 mm (0.0157, 0.0236, 0.0315, 0.0394, 0.0551, 0.0709, 0.0787, 0.0984, 0.118, 0.157, 0.177, 0.217, 0.236, 0.276, and 0.315 in.). The displacement protocol, shown in Fig. 6, was developed based on the results obtained from VecTor2¹⁸ analysis to capture complete behavior of the walls under the reverse cyclic loading. For each displacement, two complete cycles were applied. The lateral load excursions

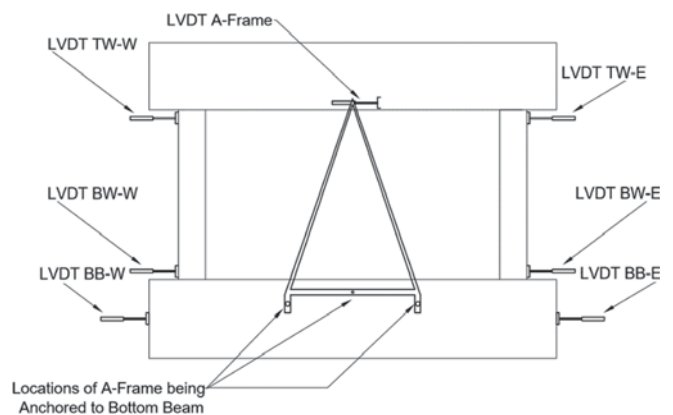


Fig. 5—Instrumentation of wall.

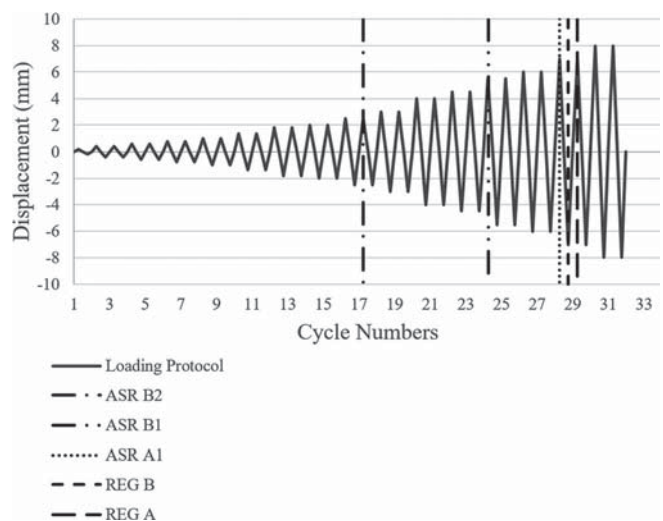


Fig. 6—Loading protocol. (Note: 1 mm = 0.0394 in.)

were continued until a significant drop in the axial load was noted and the walls could not maintain the axial load capacity. From that point forward, the wall was pushed monotonically until the complete failure. Failure point was considered where the shear wall was no longer capable of taking 40% of applied axial load.

Loading protocol provided was used as a general guidance during the structural testing. This loading protocol was based on the pretesting finite element analysis. However,

Table 2—Summary of test results

Wall	Age, days	Concrete compressive strength, MPa (ksi)	ASR free expansion, %	Peak force, kN (kip)	Maximum displacement, mm (in.)	Mode of failure
REG A	240	79.0 (11.5)	0.0329	1180 (265)	8.2 (0.322)	Diagonal shear with sliding between wall panel and the bottom beam at end
REG B	975	80.1 (11.6)	0.0331	1187 (267)	7.3 (0.287)	
ASR A1	260	63.7 (9.2)	0.19	1355 (305)	7.1 (0.280)	Diagonal shear
ASR B1	610	67.1 (9.7)	0.215	1240 (279)	4.9 (0.193)	Diagonal shear
ASR B2	995	63.0 (9.1)	0.223	1243 (280)	2.6 (0.102)	Diagonal shear

during the test, in some circumstances, this protocol had to be modified due to equipment problems, human error, and other factors such as unique behavior of each wall.

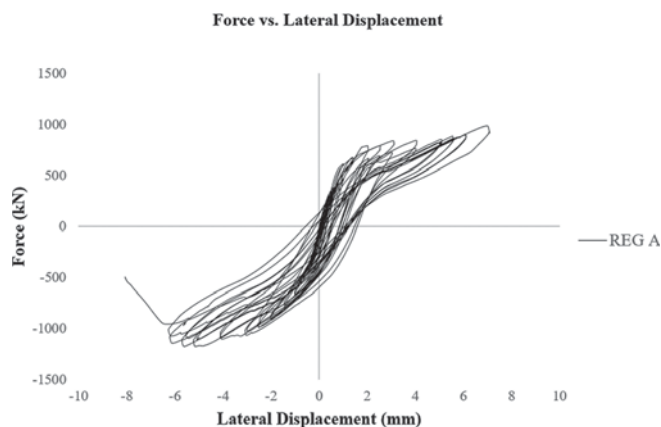
EXPERIMENTAL RESULTS AND DISCUSSION

Wall behavior

A summary of results from the structural testing of five shear walls is presented in Table 2. It must be noted that the expansion values, which are reported for each specimen, were measured on plain concrete prisms according to ASTM C1293.¹⁷ The force applied on the wall was determined from the load cells in the actuators. The lateral displacement along the height of the specimen from bottom beam to the top beam on both sides of the specimen was obtained using seven LVDTs.

In Fig. 7, lateral force-lateral displacement relations for shear walls REG A and REG B are shown. Between these two walls, the only variable is their age and duration for which these walls were cured. REG A was tested at the age of 240 days while REG B was tested after 995 days of casting. Both walls displayed similar hysteretic responses. The peak load of wall REG A was measured as 1180 kN (265 kip) with the corresponding lateral displacement of 8.2 mm (0.322 in.), while REG B shear wall had a capacity of 1187 kN (267 kip) at a lateral displacement of 7.3 mm (0.287 in.). By comparing the force-lateral displacement responses of the three ASR walls shown in Fig. 8, their degradation over time can be clearly observed. It should be noted that walls ASR A1, ASR B1, and ASR B2 were tested 260, 610, and 995 days after casting. The time of curing in the control chamber is 52 days less than the wall age.

ASR A1, which was tested 260 days after casting, displayed shear strength of 1355 kN (305 kip). At the age of 610 days, the shear capacity of wall ASR B1 was measured to be 1240 kN (279 kip). The last shear wall in the ASR category was ASR B2, which was tested 995 days after casting, showed the peak shear strength of 1243 kN (280 kip). Although the concrete compressive strength of specimen ASR B1 was greater than that in ASR B2, both specimens had approximately the same shear strength. Also, the initial stiffness of the walls and loss of stiffness in cycles beyond the peak strength are similar. In cycles, close to where the maximum peak strength is attained and cycles beyond this point, significantly large cracks started opening up horizontally along the bottom of the shear panel of the regular walls, resulting in slight pinching in the hysteresis loops. Small lift-off at the base of the walls from the ground was noticed close to the end of all the tests and it was measured to be



(a)



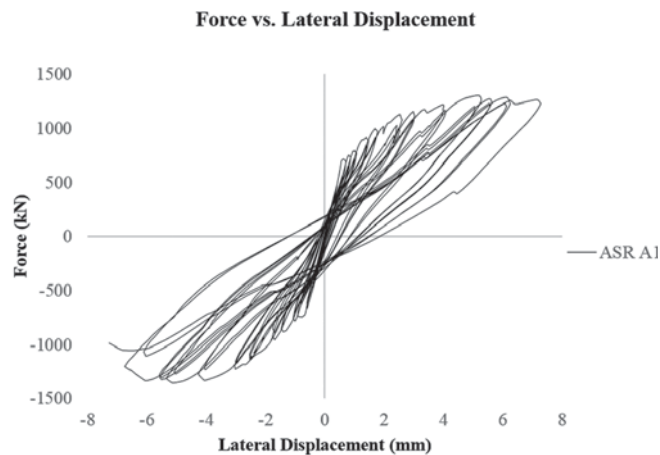
(b)

Fig. 7—Hysteresis responses of: (a) REG A; and (b) REG B shear walls. (Note: 1 kN = 0.225 kip; 1 mm = 0.0394 in.)

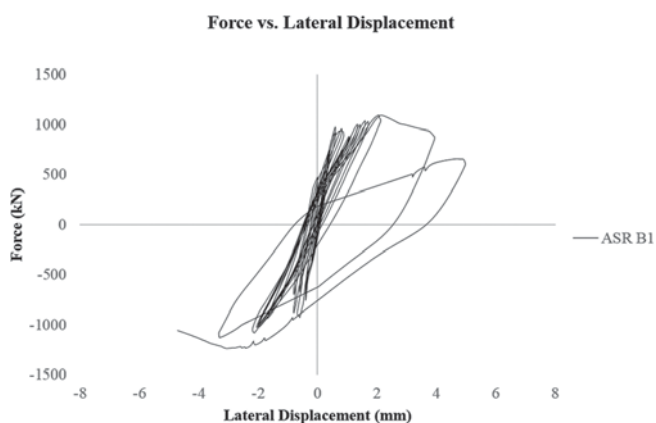
between 0.5 and 0.75 mm (0.02 and 0.03 in.) accompanied by vertical cracks in the bottom beams.

Crack patterns

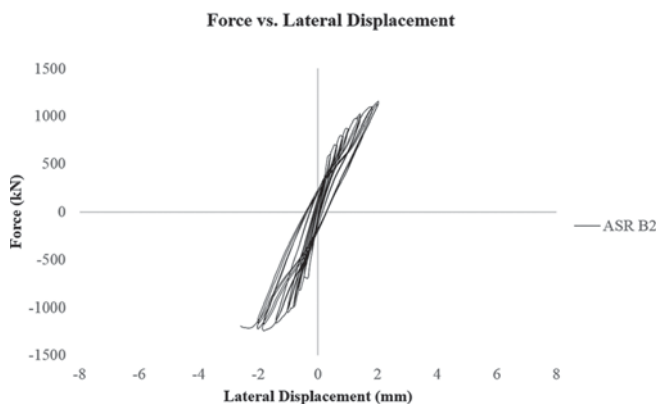
Crack patterns for all the shear walls were quite similar for most of the duration of testing. Diagonal shear cracks appeared on the shear wall panel as the test was proceeding. However, overall, ASR shear walls showed narrower cracks compared to those in the regular shear walls up until the middle stages of the structural testing. At that stage (60% of the maximum lateral displacement), large cracks were noticed initiating on the boundary elements of both ASR and regular shear walls. From this stage onward, the spacing between the cracks in ASR shear walls reduced while cracks became wider. However, in the regular shear walls, once initiated, cracks maintained their spacing as they were becoming



(a)



(b)



(c)

Fig. 8—Hysteresis responses of: (a) ASR A1; (b) ASR B1; and (c) ASR B2 shear walls. (Note: 1 kN = 0.225 kip; 1 mm = 0.0394 in.)

wider. In late stages of the testing (85% of maximum lateral displacement), crushing of the concrete was noticed on the bottom of the boundary elements as well as in the panel close to bottom beams for regular shear walls, as highlighted in Fig. 9(a). At this point, large cracks and spalling of the concrete initiated at the bottom of the panel parallel to the bottom beam. These cracks eventually led to the failure of the regular shear walls, as shown in Fig. 9(b). On the other hand, ASR shear walls did not show any sign of spalled

concrete on the boundary elements or shear wall panel along and close to the bottom beam until very late stages of the test, just before failure. In ASR shear walls, large diagonal cracks resulted in the failure as shown in Fig. 9(c) and 9(d).

Strain gauge results

Strain gauge data from Phase 1 of the structural testing revealed that reinforcing bars behaved differently in regular and ASR shear walls. In the regular wall, first vertical reinforcement in the boundary element of the tension side, started to yield at approximately 1.95 mm (0.0768 in.) of lateral displacement. At lateral displacement of 5 mm (0.2 in.), all the vertical reinforcements in the boundary element of the tension side yielded. In the shear wall panel, only three vertical reinforcing bar close to the boundary elements yielded at later stage of the testing. However, none of the horizontal reinforcing bars yielded until a lateral displacement of approximately 7 mm (0.28 in.) was achieved. Just before failure, the two horizontal reinforcing bars close to the bottom beam experienced yielding. In the ASR A1 shear wall, vertical reinforcements in the boundary element experienced yielding at approximately 1.35 mm (0.0531 in.) of lateral displacement. Eventually, all the vertical reinforcement in the boundary element of the tension side yielded at 3.5 mm (0.14 in.) of the lateral displacement. As displacement cycles were progressing, more vertical reinforcing bars in the wall panel were yielding. All the vertical reinforcing bars in the shear wall panel yielded at lateral displacement of 5.5 mm (0.22 in.). At this stage, vertical bars in the boundary elements were experiencing large plastic deformations. Horizontal reinforcing bars in the ASR A1 wall panel started to yield at a lateral displacement of approximately 3 mm (0.12 in.). At lateral displacement of 5 mm (0.2 in.), almost all the horizontal bars in the shear wall panels yielded. ASR expansion caused the reinforcing bars in ASR walls to experience prestraining before the structural testing. Also, due to the existence of microcracks and lower tensile capacity of concrete in ASR walls, reinforcing bars were engaged at an earlier stage of loading. As mentioned previously, dependable strain gauge data are not available for the walls tested in Phase 2 and Phase 3 due to the damage experienced by strain gauges over time in the accelerating chamber.

Shear capacity

The ultimate shear capacity of the walls was not significantly affected due to the type of aggregate or the age of the walls in this study. In the low-aspect-ratio shear walls, vertical reinforcement plays a more significant role than the horizontal reinforcement and the compressive strength of the concrete in determining the maximum shear strength.^{19,20} Many codes and standards such as CSA A23.3-14⁶ neglect or minimize the contribution of the concrete shear resistance in calculating the maximum shear strength of the low-aspect shear walls. It was thus expected that all the tested walls would show similar peak shear strength because all these walls had identical vertical reinforcement ratios in both panel section and the boundary elements. In addition, heavily reinforced boundary elements in low-aspect-ratio shear walls help maintain peak shear strength at cycles of displacement

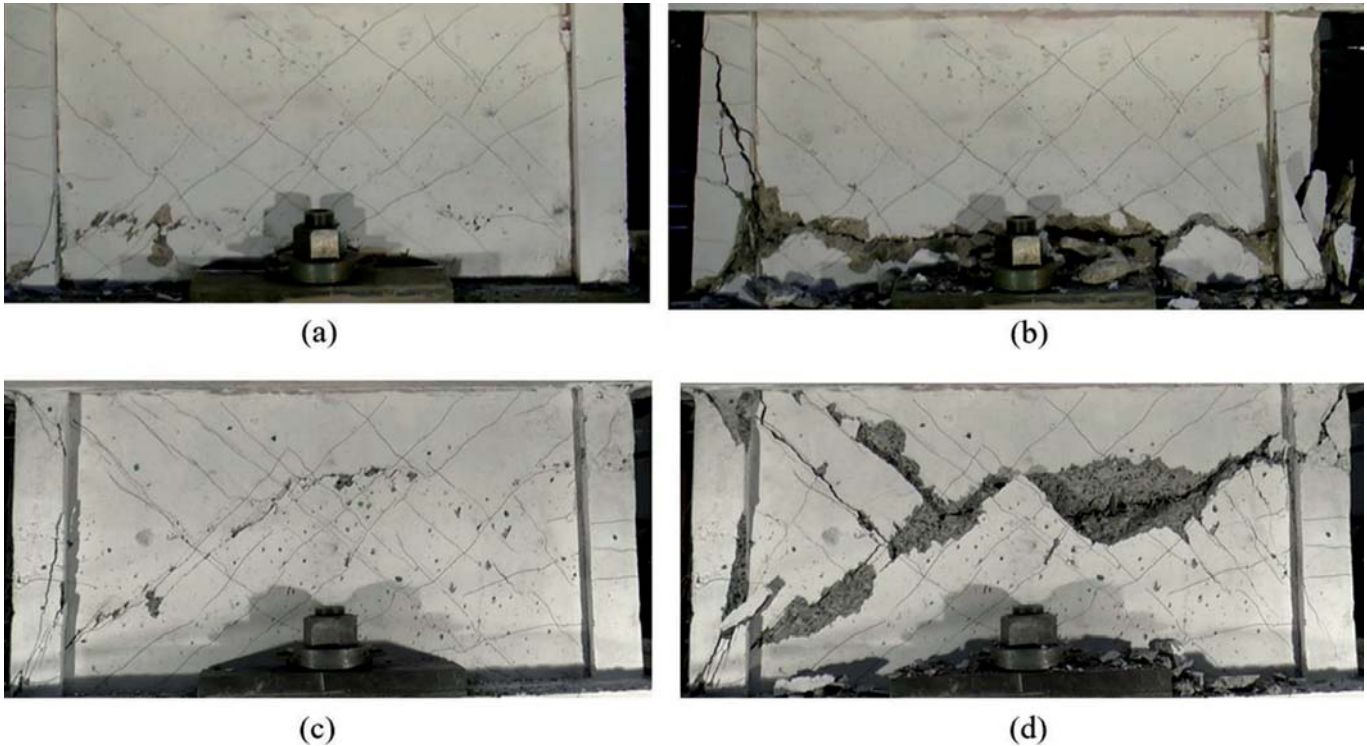


Fig. 9—Failure mechanism of: (a,b) REG B shear wall; and (c,d) ASR B2 shear wall.

beyond peak strength.²¹ As a result, similar shear degradation beyond the peak was observed in the specimens that had not sustained serious damage (such as complete debonding of reinforcing bars from concrete, spalling of cover) due to ASR.

The factored shear strength of the tested walls is calculated based on the guidelines and equations available in CSA A23.3-14,⁶ ACI 349-13,⁷ and ASCE 43-05²² and compared to the measured shear strength for each shear wall. In CSA A23.3-14,⁶ the shear resistance of the concrete is neglected. Thus, the shear capacity of the squat shear walls is solely depending on the reinforcement ratio. The angle of inclination of diagonal compressive stresses can be chosen between a maximum value of 45 degrees and a minimum of 30 degrees. Thus, the shear capacity of the wall would vary between two values. In Fig. 10, the measured and the predicted shear values using different formulations are plotted for each specimen. In this figure, CSA 30 and CSA 45 represent values using the CSA equation with the angle of inclination of diagonal compressive stresses of 30 and 45 degrees, respectively.

Significant scatter in the prediction of shear strength of the walls is noted from Fig. 10. The CSA equation provides a range of values between two limits of CSA 30 and CSA 45 based on the angle chosen. Therefore, carefully choosing the angle of inclination of diagonal compression will likely give a more accurate prediction among the compared codes. The ACI procedure⁷ provides an unconservative estimate of the peak shear strength with up to 17% overstrength. Among the methods evaluated, the ASCE procedure²² significantly overestimated the peak shear strength.

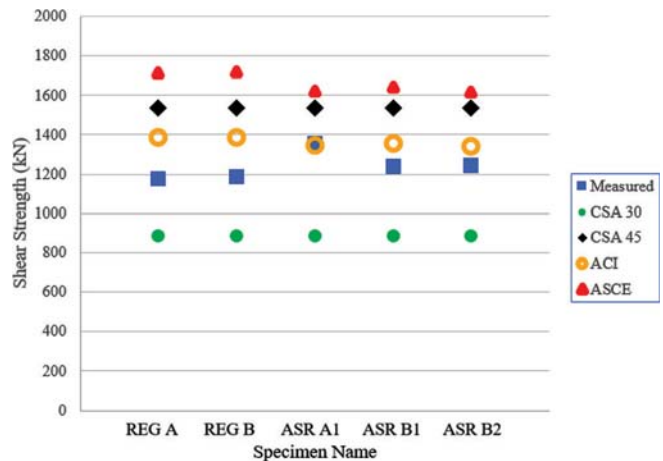


Fig. 10—Shear strength comparison between different codes and experiment. (Note: 1 kN = 0.225 kip.)

Post-peak response

The post-peak response and ductility performance of the wall would generally depend on the horizontal reinforcement and the bond between the bars and concrete. REG A and REG B shear walls showed similar behavior, including the peak shear load and the ultimate lateral displacement. The reduced lateral displacement of wall REG B may be due to slightly higher stiffness of concrete and some deterioration of bond between the horizontal reinforcement in the panel and the concrete over time. While peak shear strengths of five walls were similar, hysteresis responses of shear walls showed significant differences in their performance. Figure 6 shows the maximum lateral displacement of each specimen with respect to the loading protocol. Vertical lines in Fig. 6 show the cycle numbers at which different test specimens failed to continue resisting the applied axial

load. Subsequently, the walls were pushed monotonically to the failure.

To compare the ductility of the walls, parameters such as strain energy absorption and ductility factor of each wall from their hysteresis responses were calculated. The total amount of energy that had been imposed on the test specimen was calculated as the sum of areas enclosed under the load-displacement curves for each cycle. Equation (1) was used to obtain the external work done on a specimen

$$W = \sum_{i=1}^n \int P_i \cdot d\delta_i \quad (1)$$

where n is the number of cycles; P is applied load; and δ is displacement in the loading direction.

Because the tests were carried out with a slow rate of loading, the kinetic energy and any viscous damping can be neglected. Therefore, the external work done on the specimen can be assumed to be equal to the strain energy absorbed by the specimen.

Another way to characterize the shear walls for their ability to deform is to calculate the displacement ductility factor. This parameter is defined as

$$\mu_{\Delta} = \frac{\Delta_u}{\Delta_y} \quad (2)$$

where Δ_u is ultimate displacement at a point when the applied axial load reduced by 60%; and Δ_y is yield displacement.

The ultimate displacement is referred to the maximum displacement that the shear wall experienced before the failure. The yield displacement was defined as the lateral displacement of the shear wall at which the outermost vertical reinforcement yielded in any of the boundary elements. Table 3 shows the strain energy capacity and ductility factors for each specimen.

As shown in Table 3, the energy absorption capacity and the displacement ductility factor of the ASR shear walls reduced significantly with time as the walls were aging in the curing chamber. ASR shear wall A1 was the most ductile wall among all the walls tested, even though its ultimate lateral displacement was lower than the maximum displacements experienced by REG A and REG B shear walls. As seen previously in the hysteresis behavior of the walls, at early ages, the ASR shear walls showed better performance compared to the regular shear walls. For instance, ASR A1 showed higher peak shear strength and higher energy capacity compared to REG A. Both these walls were tested in Phase 1. It was postulated that factors such as confinement and prestressing of reinforcement due to ASR expansion affected the ultimate capacity of the ASR shear wall that was approximately 14% higher than that of the regular shear wall specimen. At this stage, steel bars in the ASR A1 wall in both vertical and horizontal directions were prestressed to a certain degree due to the internal expansion of the concrete. As a result, a stiffer behavior of this wall was observed compared to REG A shear wall. This also resulted in ASR A1 experiencing a higher peak shear strength and better ductility response. In both regular shear walls, A and B, the

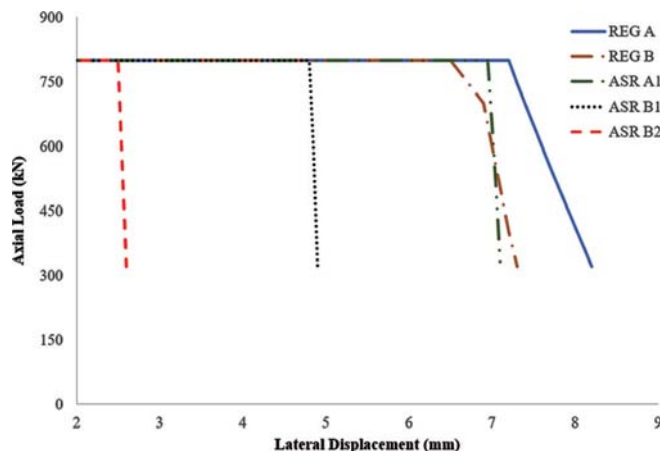


Fig. 11—Axial load versus lateral displacement. (Note: 1 kN = 0.225 kip; 1 mm = 0.0394 in.)

Table 3—Ductility behavior of shear walls

Wall	Displacement at yielding point, mm (in.)	Displacement ductility factor	Absorbed strain energy, J
REG A	1.95 (0.0768)	4.21	31,081
REG B	1.80 (0.0709)	4.06	28,759
ASR A1	1.35 (0.0531)	5.26	37,766
ASR B1	1.30 (0.0512)	3.77	17,278
ASR B2	0.90 (0.0354)	2.89	7183

Table 4—Axial load drop rate

Specimen	REG A	REG B	ASR A1	ASR B1	ASR B2
Axial drop rate, kN/mm (kip/in.)	-460 (-2628)	-807 (-4612)	-2940 (-16,802)	-4150 (-23,717)	-4820 (-27,546)

axial load was maintained by the specimens up to the failure and gradually decreased after the failure initiated and the base of the wall panel slid from the bottom beam. In contrast, the drop of axial load in the ASR walls was relatively sudden and the specimens failed with little to no warning at the failure point, showing diagonal cracking in the panel. This most likely is due to the degradation of the ASR concrete properties such as modulus of elasticity and tensile strength. Figure 11 shows the axial load versus displacement response of each shear wall specimen.

To compare the rate at which the axial load dropped, the slope of axial drop was calculated and is presented in Table 4 for each specimen. It is obvious that ASR specimens in general showed much brittle behavior compared to the regular shear walls.

As the walls were aging, it was noticed that the performance of the regular shear wall from REG A to REG B did not change significantly. On the other hand, performance of ASR B2 showed a significant reduction of performance in terms of maximum lateral displacement and capacity to absorb the strain energy compared to ASR A1 and B1. Even though the expansion measured on the concrete prisms showed only 17% more expansion between ASR A1 (Phase 1) and ASR B2 (Phase 3), the energy absorption capacity of ASR B2 was

reduced by over 80%. The plausible reasons for this notable reduction are discussed in the following.

First, the expansion values shown were measured from plain concrete prisms with no restraints. Concrete in these specimens expanded almost freely and reached its exhaustion level at its own rate. Shear walls contained a significant amount of reinforcement that provided restraint to the expansion of concrete caused by ASR. Moreover, boundary elements—top and bottom beams—added extra confinement to the shear wall panel, restraining this panel further from free expansion. As a result, the rate of expansion in the shear wall is expected to be slower than that in the plain concrete prisms, and the concrete at least in the earlier stages would be confined significantly.

Second, although given little attention, one of the adverse effects of ASR in reinforced concrete is the deterioration of bond between the reinforcing bars and the concrete. Beside the actual nature of the ASR expansion, which may cause debonding between concrete and reinforcing bars, cracks and openings in the concrete further weakens the bond. The vertical reinforcing bars were anchored in the large beams at the top and the bottom. Horizontal bars, however, did not have similar anchoring and, thus, were more vulnerable to debonding from concrete due to ASR. A series of pullout tests have shown that the ultimate bond strength between the concrete and steel reinforcing bar was reduced by approximately 24% in specimens made by ASR.²³ To predict the long-term behavior of structures affected by ASR, a thorough investigation is underway at the University of Toronto to better understand the effect of ASR on bond strength in reinforced concrete.

Furthermore, the shear walls were constantly exposed to moisture and circulated air, and had small clear cover of 34 mm (1.34 in.) to steel. As a result, some corrosion was observed in the last specimen tested (ASR B2). The effect of corrosion on the performance of the shear walls requires further investigation which was beyond the scope of this project. Figure 12 shows the corrosion marks on the reinforcing bars exposed after testing in one location of the ASR B2 specimen. In real structures exposed to the atmospheric environment, other factors such as freezing and thawing can also significantly accelerate the damage to the structure.

SUMMARY AND CONCLUSIONS

To understand the effect of ASR on reinforced concrete, results from five squat shear walls are presented. Three walls were constructed using ASR concrete and two with regular concrete. All the walls and associated smaller specimens were stored in a chamber 48 days after they were constructed and maintained in the chamber until testing. The high-temperature and high-humidity chamber was maintained at 50°C (122°F) and over 95% relative humidity. The walls were tested under reverse cyclic displacement excursions while subjected to a constant axial load at three different ages. Based on the results of this experimental program, the following conclusions can be drawn:

1. At an early age (240 days after casting), initial stiffness and ultimate strength of the ASR shear wall were higher than those of the regular wall. This is likely due to confine-

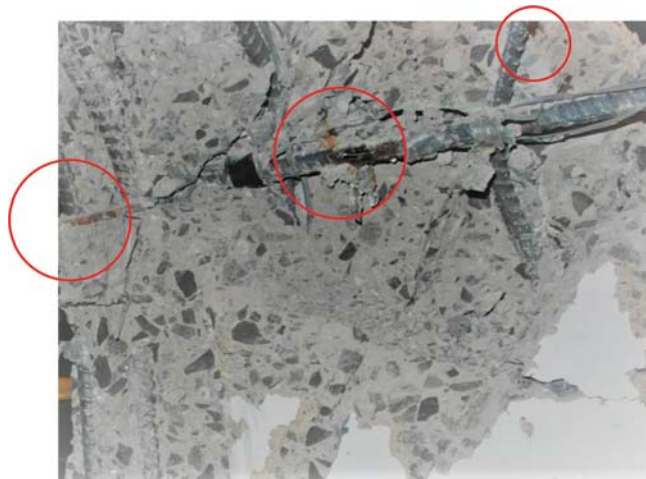


Fig. 12—Corrosion spotted on reinforcing bars.

ment and prestressing of internal reinforcement due to ASR expansion.

2. There is a noticeable scatter in predicted shear strength of squat shear walls calculated using CSA, ACI, and ASCE formulations. CSA seems to capture the actual peak shear strength values obtained from the test by choosing the correct angle of inclination of diagonal compression. Both ACI and ASCE overestimate the peak shear strength for the shear walls tested.

3. Shear capacity of the shear walls is mostly determined by the amount of available vertical reinforcement. Because vertical bars were sufficiently anchored in large beams at the top and the bottom, the ultimate shear capacity of the shear walls was not significantly affected by the adverse effect of the ASR. However, the horizontal bars did not have the same anchorage condition. Thus, expansion caused by ASR resulted in a significant deterioration of the wall's behavior with respect to energy absorption and displacement ductility over time. The absorbed strain energy and ductility factor of the last ASR wall tested reduced to approximately 20% and 55%, respectively, compared to the similar wall tested earlier, while the same parameters for the regular walls did not change significantly.

4. ASR shear walls lost their ability to maintain the axial load rapidly and failed in a sudden manner under lateral displacement excursions whereas in regular wall specimens, the axial load resistance dropped more gradually and the failure was not as sudden.

5. The expansion mechanism due to ASR in plain concrete does not accurately represent the phenomenon of ASR expansion in reinforced concrete. Depending on the boundary conditions—the amount and the arrangement of the reinforcement—deterioration of the concrete properties could be compensated by the stressing of the reinforcing bars due to ASR expansion and the resulting concrete confinement.

6. Factors such as steel corrosion, increased susceptibility to freezing and thawing, and debonding between steel bars and concrete could potentially affect the behavior of structures built with ASR concrete in an adverse manner. Further studies are thus needed to investigate these effects.

AUTHOR BIOS

Farhad Habibi is a PhD Candidate in the Department of Civil Engineering at the University of Toronto, Toronto, ON, Canada. He received his bachelor's degree in civil engineering from McMaster University, Hamilton, ON, Canada. His research interests include investigation of reinforced concrete structures affected by alkali-silica reaction (ASR), seismic design of structures, finite element analysis of structures, and monitoring and evaluating life expectancy of the reinforced concrete structures.

Shamim A. Sheikh, FACI, is a Professor of civil engineering at the University of Toronto. He is a member and past Chair of Joint ACI-ASCE Committee 441, Reinforced Concrete Columns, and a member of ACI Committee 374, Performance-Based Seismic Design of Concrete Structures. He received the ACI Structural Research Award in 1999. His research interests include earthquake resistance and seismic upgrade of concrete structures, confinement of concrete, and use of fiber-reinforced polymers in concrete structures.

Frank J. Vecchio, FACI, is a Professor of civil engineering at the University of Toronto. He is a member of Joint ACI-ASCE Committees 441, Reinforced Concrete Columns, and 447, Finite Element Analysis of Concrete Structures. He received the ACI Structural Research Award in 1998, the ACI Structural Engineering Award in 1999, the Wason Medal for Most Meritorious Paper in 2011, and the Joe Kelly Award in 2016. His research interests include advanced constitutive modeling, assessment and rehabilitation of concrete structures, and response under extreme load conditions.

ACI member **Daman K. Panesar** is an Associate Professor in the Department of Civil Engineering at the University of Toronto. Her research interests include advancing concrete materials, low-carbon materials, material characterization, and durability performance of aging infrastructure.

ACKNOWLEDGMENTS

The authors wish to express their gratitude to the Canadian Nuclear Safety Commission (CNSC) for funding this research. The experimental work was carried out in the Structures Laboratories of the University of Toronto. This paper represents the opinion of the authors and is not the technical position of CNSC.

REFERENCES

1. U.N. Commission, "Safety Evaluation Report with Open Items related to the Licence Renewal of Seabrook Station," U.S. Nuclear Regulatory Commission, Rockville, MD, 2012, 766 pp.
2. Kobayashi, K.; Inoue, S.; Yamasaki, T.; and Nakano, K. I., "Alkali Aggregate Reaction in Prestressed Concrete Beams," *International Journal of Cement Composites and Lightweight Concrete*, V. 10, No. 4, 1988, pp. 233-240. doi: 10.1016/0262-5075(88)90053-X
3. Fan, S., and Hanson, J. M., "Effect of Alkali-Silica Reaction Expansion and Cracking on Structural Behavior of Reinforced Concrete Beams," *ACI Structural Journal*, V. 95, No. 5, Sept.-Oct. 1998, pp. 498-505.
4. Deschenes, D. J.; Bayrak, O.; and Folliard, K. J., "ASR/DEF – Damaged Bent Caps: Shear Tests and Field Implications," Technical Report No. 12-8XXIA006, Texas Department of Transportation, Austin, TX, 2009, 271 pp.
5. Bouchon, M.; Orbovic, N.; and Foure, B., "Tests on Reinforced Concrete Low-Rise Shear Walls under Static Cyclic Loading," Thirteenth World Conference on Earthquake Engineering, Vancouver, BC, Canada, 2004, 11 pp.
6. CSA A23.3-14, "Design of Concrete Structures," Canadian Standard Association, Mississauga, ON, Canada, 2014.
7. ACI Committee 349, "Code Requirements for Nuclear Safety Related Concrete Structures (ACI 349-13) Commentary," American Concrete Institute, Farmington Hills, MI, 2013, 196 pp.
8. Ichikawa, T., and Miura, M., "Modified Model of Alkali-Silica Reaction," *Cement and Concrete Research*, V. 37, No. 9, 2007, pp. 1291-1297. doi: 10.1016/j.cemconres.2007.06.008
9. Pan, J. W.; Feng, Y. T.; Wang, J. T.; Sun, Q. C.; Zhang, C. H.; and Ownen, D. R. J., "Modeling of Alkali-Silica Reaction in Concrete: A Review," *Frontiers of Structural and Civil Engineering*, V. 6, No. 1, 2012, pp. 1-18.
10. Gautam, B., "Multiaxially Loaded Concrete Undergoing Alkali Silica Reaction," PhD thesis, University of Toronto, Toronto, ON, Canada, 2016, 187 pp.
11. ASTM C1293-08b(2015), "Standard Test Method for Determination of Length Change of Concrete due to Alkali-Silica Reaction," ASTM International, West Conshohocken, PA, 2015, 7 pp.
12. CSA A23.2-14A, "Potential Expansivity of Aggregates (Procedure for Length Change due to Alkali-Aggregate Reaction in Concrete Prisms at 38°C)," Canadian Standard Association, Mississauga, ON, Canada, 2009, pp. 350-362.
13. RILEM TC 106-AAR, "Detection of Potential Alkali-Reactivity of Aggregates — Method for Aggregate Combinations Using Concrete Prisms (B-TC 106-3)," *Materials and Structures*, V. 33, June 2000, pp. 290-293.
14. Fournier, B.; Chevrier, R.; de Grosbois, M.; Lisella, R.; Folliard, K.; Ideker, J.; Shehata, M.; Thomas, M.; and Baxter, S., "The Accelerated Concrete Prism Test (60°C): Variability of the Test Method and Proposed Expansion Limits," 12th International Conference on Alkali Aggregate Reaction, Beijing, China, 2004, 10 pp.
15. Thomas, M.; Fournier, B.; Folliard, K.; Ideker, J.; and Shehata, M., "Test Methods for Evaluating Preventive Measures for Controlling Expansion due to Alkali-Silica Reaction in Concrete," *Cement and Concrete Research*, V. 36, No. 10, 2006, pp. 1842-1856. doi: 10.1016/j.cemconres.2006.01.014
16. Ideker, J. H.; East, B. L.; Folliard, K. J.; Thomas, M. D. A.; and Fournier, B., "The Current State of the Accelerated Concrete Prism Test," *Cement and Concrete Research*, V. 40, No. 4, 2010, pp. 550-555. doi: 10.1016/j.cemconres.2009.08.030
17. Folliard, K.; Ideker, J.; Thomas, M. D. A.; and Fournier, B., "Assessing Aggregate Reactivity Using the Accelerated Concrete Prism Test," *Proceedings of the Seventh CANMET/ACI International Conference on Recent Advances in Concrete Technology*, SP-222, American Concrete Institute, Farmington Hills, MI, 2004, pp. 269-283.
18. Wong, P. S.; Vecchio, F. J.; and Trommels, H., *VecTor2 and FormWorks User's Manual*, University of Toronto, Toronto, ON, Canada, 2013, 318 pp.
19. Gulec, C. K., "Empirical Equations for Peak Shear Strength of Low Aspect Ratio Reinforced Concrete Walls," *ACI Structural Journal*, V. 108, No. 1, Jan.-Feb. 2011, pp. 80-89.
20. Barda, F.; Hanson, J. M.; and Corley, W. G., "Shear Strength of Low-Rise Walls with Boundary Elements," *Reinforced Concrete Structures in Seismic Zones*, SP-53, N. M. Hawkins and D. Mitchell, eds., American Concrete Institute, Farmington Hills, MI, 1977, pp. 149-202.
21. Luna, B. L.; Rivera, J. P.; and Whittaker, A. S., "Seismic Behavior of Low-Aspect-Ratio Reinforced Concrete Shear Walls," *ACI Structural Journal*, V. 112, No. 5, Sept.-Oct. 2015, pp. 593-603. doi: 10.14359/51687709
22. ASCE/SEI 43-05, "Seismic Design Criteria for Structures, Systems, and Components in Nuclear Facilities," American Society of Civil Engineers, Reston, VA, 2005, pp. 52-62.
23. Haddad, R. H., and Numayr, K. S., "Effect of Alkali-Silica Reaction and Freezing and Thawing Action on Concrete-Steel Bond," *Construction and Building Materials*, V. 21, No. 2, 2007, pp. 428-435.